Epitaxially Grown Layered MFI–Bulk MFI Hybrid Zeolitic Materials

Wun-gwi Kim,[†] Xueyi Zhang,[‡] Jong Suk Lee,[†] Michael Tsapatsis,[‡] and Sankar Nair[†,*]

[†]School of Chemical & Biomolecular Engineering, Georgia Institute of Technology, Atlanta, Georgia 30332, United States and [‡]Department of Chemical Engineering and Materials Science, University of Minnesota, Minneapolis, Minnesota 55455, United States

ABSTRACT The synthesis of hybrid zeolitic materials with complex micropore–mesopore structures and morphologies is an expanding area of recent interest for a number of applications. Here we report a new type of hybrid zeolite material, composed of a layered zeolite material grown epitaxially on the surface of a bulk zeolite material. Specifically, layered (2-D) MFI sheets were grown on the surface of bulk MFI crystals of different sizes (300 nm and 10 μm), thereby resulting in a hybrid material containing a unique morphology of interconnected micropores (~0.55 nm) and mesopores (~3 nm). The structure and morphology of this material, referred to as a "bulk MFI–layered MFI" (BMLM) material, was elucidated by a combination of XRD, TEM, HRTEM, SEM, TGA, and N_2 physisorption techniques. It is conclusively shown that epitaxial growth of the 2-D layered MFI sheets occurs in at least two principal crystallographic directions of the bulk MFI crystal and possibly in the third direction as well. The BMLM material combines the properties of bulk MFI (micropore network and mechanical support) and 2-D layered MFI (large surface roughness, external surface area, and mesoporosity). As an example of the uses of the BMLM material, it was incorporated into a polyimide and fabricated into a composite membrane with enhanced permeability for CO_2 and good CO_2/CH_4 selectivity for gas separations. SEM-EDX imaging and composition analysis showed that the polyimide and the BMLM interpenetrate into each other, thereby forming a well-adhered polymer/particle microstructure, in contrast with the defective interfacial microstructure obtained using bare MFI particles. Analysis of the gas permeation data with the modified Maxwell model also allows the estimation of the effective volume of the BMLM particles, as well as the CO_2 and CH_4 gas permeabilities of the interpenetrated layer at the BMLM/polyimide interface.

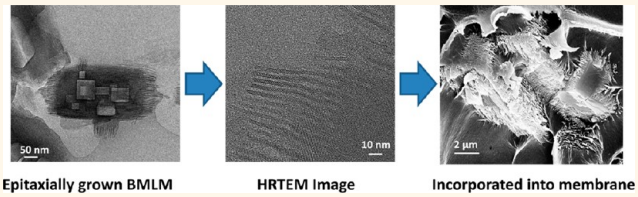

KEYWORDS: epitaxial growth · layered MFI · nanoporous materials · hybrid zeolitic materials · nanowhiskers

Zeolites are aluminosilicate materials with shape/size-selective nanopores and are widely applied in separations and catalysis.[1,2] Recent works have led to new ways of controlling molecular diffusion limitations in zeolite materials. These include the synthesis of nanosized zeolites[3] and layered and exfoliated (*i.e.*, 2-D) zeolites.[4–6] Hierarchical zeolite–mesoporous hybrid materials have also been developed to expand the applications of zeolites to handling bulky molecules such as heavy hydrocarbons and biomolecules.[7,8] The interconnected microporous and mesoporous components have complementary features: acid sites in the micropores and fast diffusion paths in the mesopores.[9,10] For example, such structures were recently obtained from ultrathin layered MFI materials.[11] Long-chain diquaternary ammonium cations ($C_{22}-N^+-C_6-N^+-C_6$) were used as templating agents to form a 2-D lamellar MFI-type material. This material was further pillared to prevent interlayer condensation during calcination.[12] Another method of preventing interlayer condensation is the synthesis of hexagonally ordered MFI/mesoporous hybrids.[13] This complex material showed interesting catalytic properties related to the existence of both micropores and mesopores. Exfoliated layered MFI was also exploited in the formation of zeolitic membranes for hydrocarbon separations.[14]

In this work, we introduce a different approach to the construction of hybrid microporous/mesoporous materials, *via* epitaxial (lattice-matched) growth of a 2-D layered zeolite on the surface of a bulk (3-D) zeolite material. There are a few demonstrations of epitaxial growth between two conventional zeolite materials, such as the growth of Zeolite-β on SSZ-31 nanofibers[15] and the growth of cancrinite on sodalite.[16] Here we report the first example of epitaxial growth of a 2-D layered zeolite (layered MFI) at the surface of a conventional zeolite

* Address correspondence to sankar.nair@chbe.gatech.edu.

Received for review August 9, 2012 and accepted October 9, 2012.

Published online October 09, 2012
10.1021/nn3036254

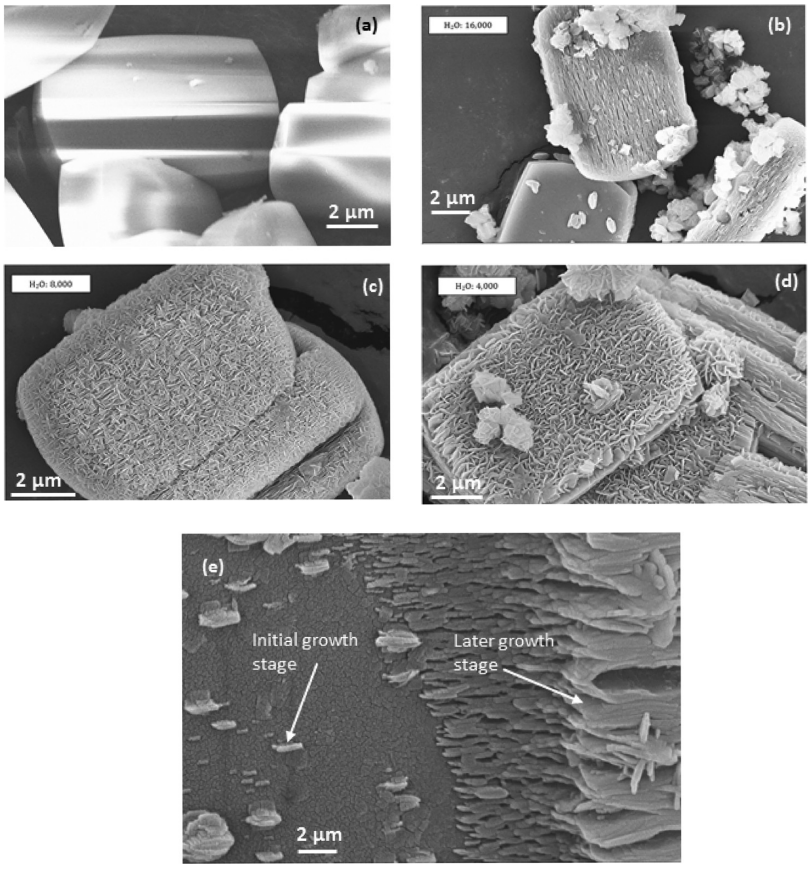

Figure 1. SEM images of (a) 10 μm bare MFI and (b–e) BMLM particles at varying water concentrations in the synthesis.

(MFI). In this hybrid material, referred to as "bulk MFI–layered MFI" (BMLM), the conventional MFI provides shape/size-selective micropores as well as condensed acid sites and acts as a support to prevent interlayer condensation and disordering of the layered MFI that otherwise occurs upon calcination. The layered component provides a combined mesoporous/microporous network and surface acid sites of controlled structure. Furthermore, control over the size of both domains (layered and bulk) can be obtained by selecting appropriate particle sizes of the bulk component and varying the epitaxial growth conditions for the layered component. In this work, we describe in detail the synthesis and characterization of this hybrid zeolite material. Furthermore, we illustrate an application of this material based upon its roughened yet highly porous surface morphology, which can be used for obtaining a high degree of zeolite–polymer adhesion during the formation of composite zeolite/polymer membranes. Other recently developed approaches for this purpose involve the growth of nanostructures of dense metal oxides/hydroxides such as $MgO/Mg(OH)_2$ on the zeolite surface.[17–19] However, the latter surface-roughened materials show variable stabilities of the surface nanostructures and reductions in porosity.[19] The BMLM-type hybrid materials are shown to avoid these problems.

RESULTS AND DISCUSSION

The morphology and structure of layered MFI was found to be identical to that reported previously.[11] Figure S1 (Supporting Information) shows the scanning electron microscopy (SEM) images of the synthesized layered MFI, which displays high-aspect-ratio platy structures aggregated with each other. Therefore, the surface morphology of the layered MFI aggregate is highly roughened. The XRD patterns (Figure S2) show the crystal structure of layered MFI. The XRD pattern of layered MFI includes only (*h*0*l*) peaks while missing the (0*k*0) peaks, thereby representing the 2-D layered MFI. Transmission electron microscopy (TEM) images are shown in Figure S3. Layered MFI contains approximately 3 nm thin MFI layers with about 3 nm spaces between layers.

The SEM image of Figure 1a shows the surface morphology of the 10 μm bare MFI particles. Figure 1b–e shows the surface morphologies of BMLM particles grown from the bare MFI particles. Layered MFI is seen to grow at the surface of conventional MFI, and the particle surface is highly roughened after the overgrowth of layered MFI. In Figure 1b–d, it is seen that the surface morphology of the BMLM material can be controlled *via* the water concentration used in the synthesis. The thickness, extent, and roughness of the surface-grown layered MFI all increased upon

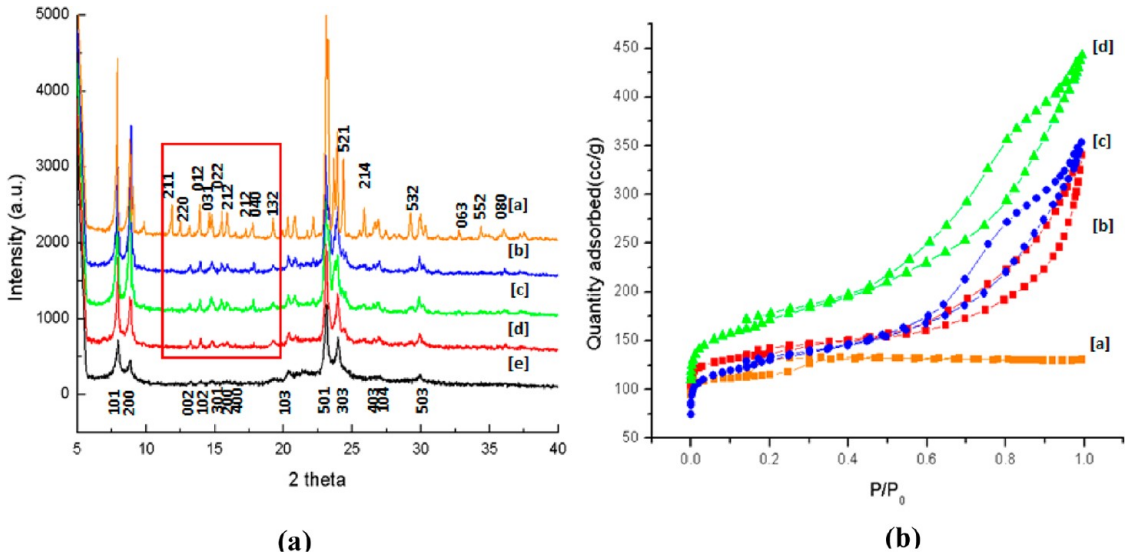

Figure 2. (a) XRD patterns of [a] bulk MFI; [b] BMLM; H_2O contents: 16 000 [c] BMLM; 8000 [d] BMLM; 4000 [e] pure layered MFI; and (b) N_2 physisorption data of [a] bulk MFI, external surface area 90 m^2/g; [b] BMLM 4000, 140 m^2/g; [c] BMLM 16 000, 236 m^2/g; [d] BMLM 8000, 308 m^2/g.

decreasing the molar ratio of water from 16 000 to 4000. Figure 1e captures different stages of growth of the layered MFI on bulk MFI. The layered MFI domains at various stages of growth all appeared to be morphologically aligned on the surface, hence suggesting an epitaxial (lattice-matched) growth rather than a more random surface deposition and overgrowth process.

Figure 2a shows XRD patterns of bulk MFI, layered MFI, and the BMLM particles. The XRD pattern of the BMLM particles includes peaks from the bulk and layered MFI materials. Figure 2b shows the N_2 physisorption isotherms and calculated *t*-plot external surface areas of bare MFI and BMLM particles. As expected from the highly roughened surface morphology of the BMLM particles in Figure 1, the mesoporosity and calculated external surface area of BMLM particles are considerably larger than in bare MFI. Depending on the water content of the reaction gel, the calculated external surface areas ranged from 140 to 308 m^2/g. On the basis of SEM and N_2 physisorption measurements, it is found that a water molar content of 8000 in the reaction gel gives the maximum roughness and external surface area.

The large (10 μm) BMLM particles were used to optimize the synthesis method, but have limitations in their application. Therefore, we extended the BMLM synthesis technique to 300 nm bulk MFI particles. A water content of 8000 was used. Figure 3a–c shows SEM images of the bulk MFI and BMLM particles. Layered MFI was successfully grown on the surface of bulk MFI, and the surface morphology was highly roughened. Figure 3d shows the N_2 physisorption characterization, corroborating the increase in surface roughness and external surface areas.

Figure 4 shows thermogravimetric traces of as-made BMLM particles, bulk MFI, and layered MFI. The organic contents of bare MFI and layered MFI were measured to be 14% and 41%, respectively, whereas the organic loading of BMLM particles was measured to be 31%. Based upon the known contents of the respective organic structure-directing agents (SDAs) in bare and layered MFI, the mass fraction of bulk MFI in BMLM particles was calculated to be 37%. The density of bulk calcined MFI is known to be 1.73 g/cm^3, and 2.05 g/cm^3 before calcination.[20] The density of as-made layered MFI is 1.544 g/cm^3. Based upon these densities, the volume fraction of bulk MFI in BMLM particles is calculated to be 30.7%. Hence, the average thickness of layered MFI on the surface of bulk MFI was calculated to be approximately 72 nm. The resulting overall average BMLM particle size of about 444 nm is comparable to the particle sizes seen in Figure 3.

Epitaxial Growth of Layered MFI in BMLM Particles. The low-resolution TEM images in Figure 5 show the cross-sectional morphology of 300 nm BMLM particles. While bare MFI shows a smooth edge (Figure 5a), the BMLM particles clearly show the growth of layered MFI at the surface of the bulk MFI particle. Furthermore, it is clear that the layered MFI grows in all three orthogonal crystallographic directions, consistent with Figure 3. The magnified image in Figure 5c demonstrates the high roughening of the MFI particle edge. One additional interesting observation in Figure 5b is the presence of well-defined rectangular "holes". This is due to selective etching of silica from the bulk MFI crystal during growth of the layered MFI.

A detailed HRTEM analysis was performed to determine if the BMLM particles represent an epitaxially grown material. Epitaxial growth can be defined as the growth of a crystalline overlayer on another crystalline substrate, with lattice matching at the interface between the two phases. In this case, it is necessary that

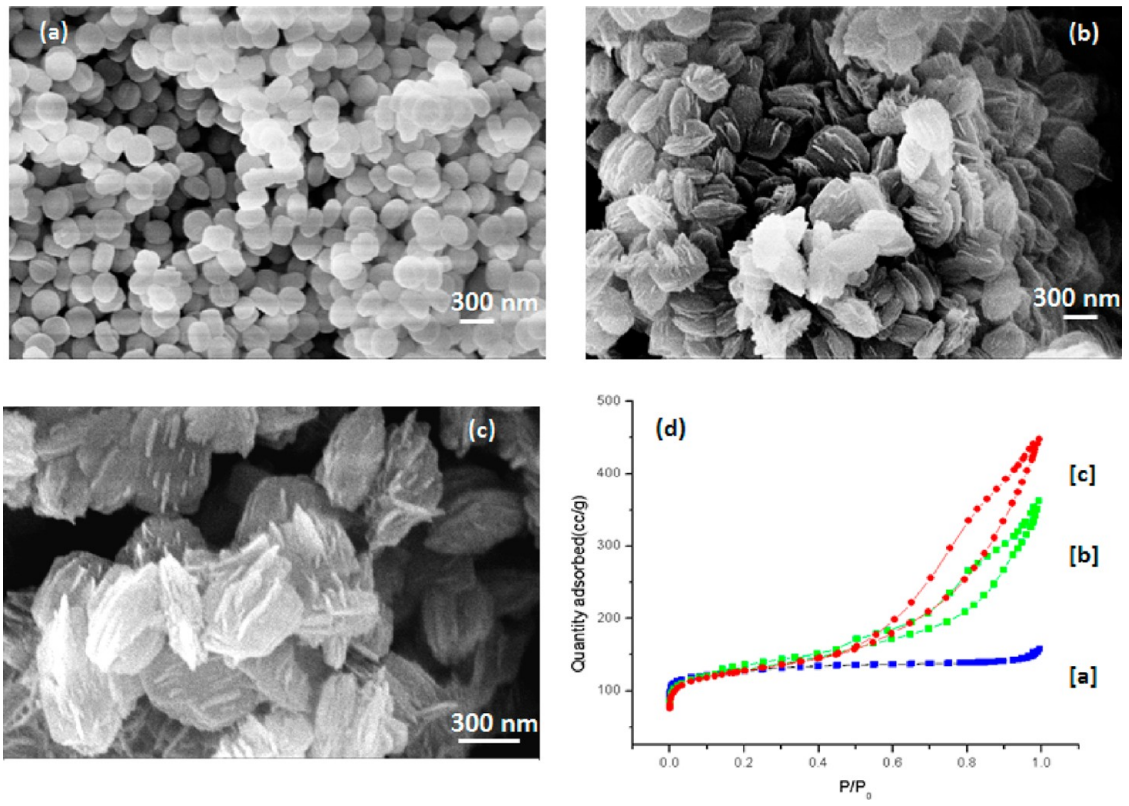

Figure 3. SEM images of (a) 300 nm bulk MFI; (b, c) BMLM particles; and (d) N_2-physisorption data of [a] 300 nm bulk MFI, external surface area = 131 m^2/g; [b] BMLM, 200 m^2/g; [c] pure layered MFI, 205 m^2/g.

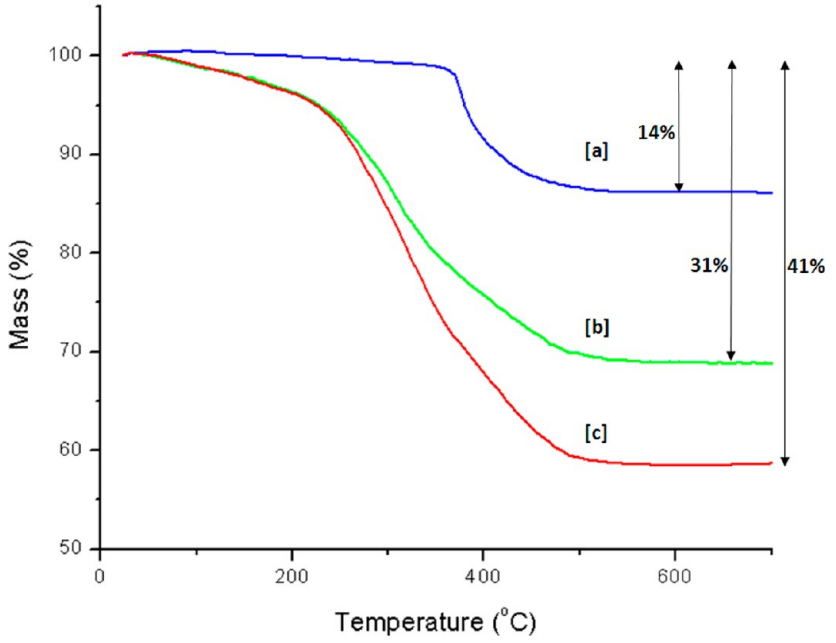

Figure 4. Thermogravimetric analysis (TGA) of [a] 300 nm bulk MFI; [b] BMLM; [c] pure layered MFI.

the crystal and pore structure of the layered MFI overgrowth be aligned with the structure of the bulk MFI substrate at the interface of the two phases. Scheme 1 shows the three possible crystal growth directions of layered MFI on bulk MFI as conjectured from the SEM images. As shown later in this report, types 1 and 2 are homoepitaxial growth in which the bulk MFI substrate and layered MFI overgrowth are along a common crystal direction. However, type 3 is a heteroepitaxial growth (or rotational overgrowth) involving twinning of the crystal directions of bulk and layered MFI.

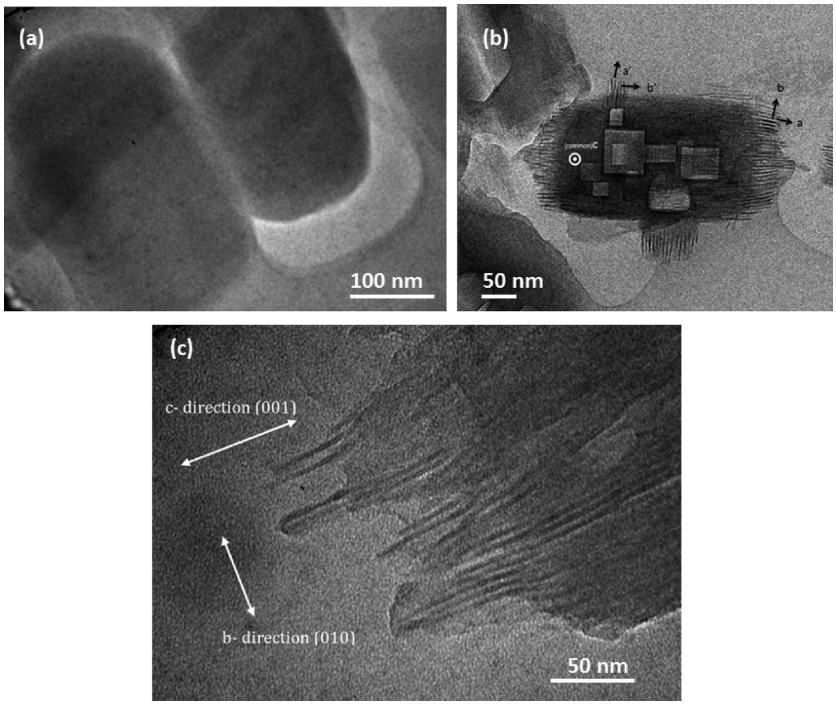

Figure 5. Low-resolution TEM images of BMLM particles.

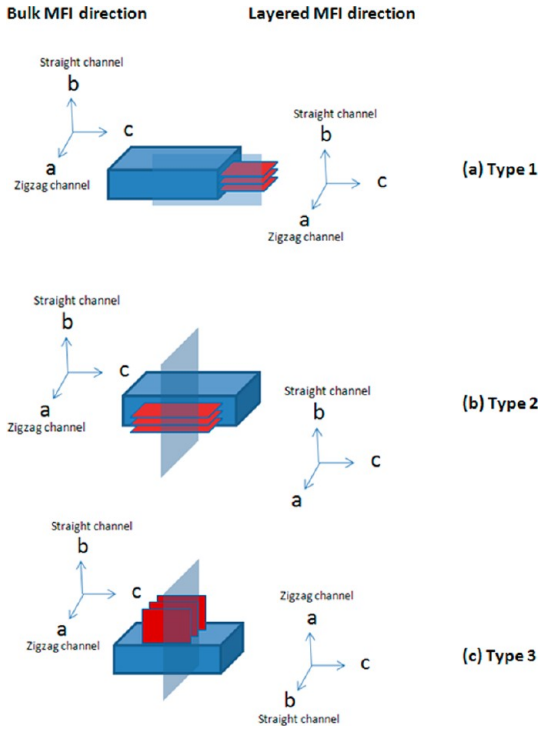

Scheme 1. BMLM morphology in three different crystal growth directions: (a) type 1: *c*-directional, (b) type 2: *a*-directional, and (c) type 3: *b*-directional growth.

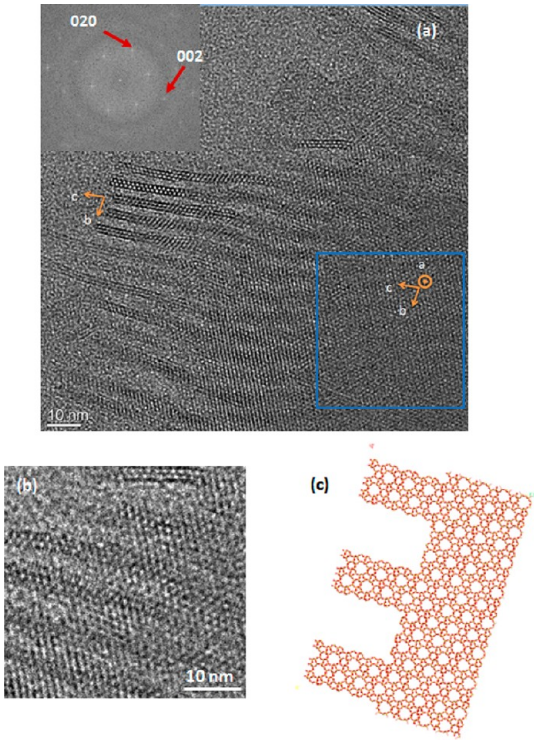

Figure 6. HRTEM analysis of BMLM epitaxial growth (type 1, *c*-direction growth).

Figures 6–8 show HRTEM images elucidating the crystal structure at the interface of BMLM particles. In all three crystal growth directions represented in these figures, both the pore structures and crystal structures of bulk MFI and layered MFI were exactly aligned, thereby representing the epitaxial growth of layered MFI at the surface of bulk MFI. The MFI pore size of 5.5 Å is clearly seen, and the pore direction in the bulk MFI region could be assigned *via* electron diffraction (ED) patterns after fast Fourier transform (FFT) of

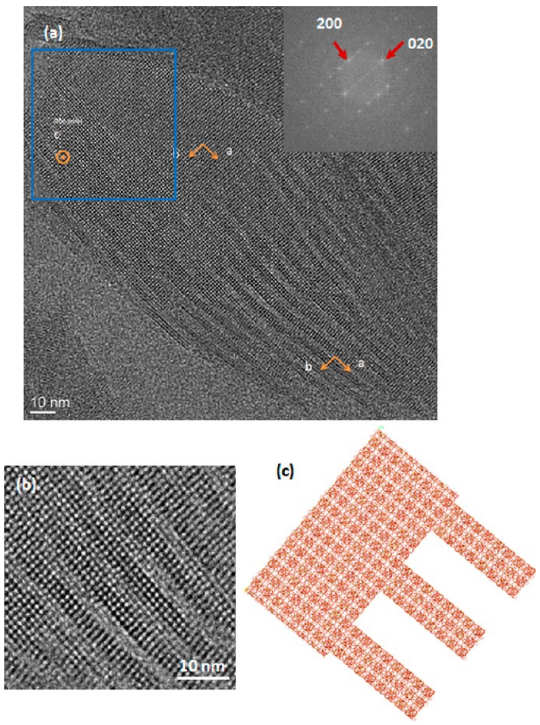

Figure 7. HRTEM analysis of BMLM epitaxial growth (type 2, *a*-direction growth).

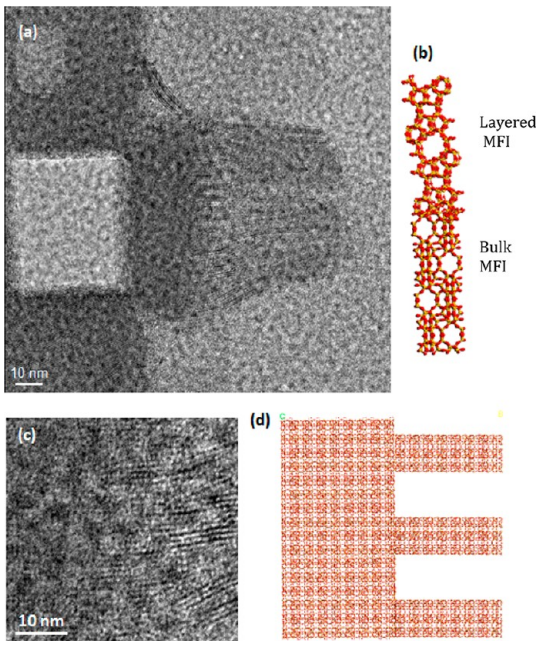

Figure 8. HRTEM analysis of BMLM epitaxial growth (type 3, *b*-direction growth).

the TEM images. Figure 6 shows the type 1 (*c*-direction) crystal growth of layered MFI, represented in Scheme 1a. The electron diffraction spots of the bulk MFI region (blue square) after FFT are indexed in the inset. The diffraction spots coincide with the actual ED pattern of bulk MFI[21] and show that the structure is being viewed down the *a*-direction pores. The magnified interfacial region in Figure 6b shows the continuity of the pore structure, as depicted by the type 1 epitaxial growth model in Figure 6c.

Figure 7 shows the interface of the type 2 (*a*-direction) crystal growth represented in Scheme 1b. The diffraction pattern of the conventional MFI region after FFT processing coincides with that of the *c*-directional MFI pore structure, due to the indexed (200) and (020) diffraction spots. The magnified pore structure in Figure 7b is used to obtain the type 2 epitaxial growth model shown in Figure 7c.

Figure 8 shows the interface of the type 3 *b*-directional crystal growth case represented in Scheme 1c. In this case, a homoepitaxial growth is not possible, and the crystal direction of layered MFI is twinned with respect to that of the bulk MFI substrate (Figure 8b and d). This rotational overgrowth occurs because the *b*-direction of layered MFI is determined by the alignment of the C_{22} long-chain hydrocarbon moiety of the SDA. However, the alignment of the C_{22} chains is perpendicular to the *b*-direction of bulk MFI. The heteroepitaxial growth hence likely occurs by a 90° rotation or twinning of the overgrown layer with respect to the substrate. Heteroepitaxial growth, as in the present BMLM type 3 case, is expected to be thermodynamically less favorable than homoepitaxial growth. It was found that the incidence of the type 3 growth was much rarer than the other two (homoepitaxial) types of growth. Due to the rarity of finding this type of growth, and the fact that there is no clearly defined pore structure available as a guideline for interpreting the HRTEM images (Figure 8d), it proved difficult to obtain a complete characterization of this growth direction. In general, the connectivity of rotational overgrowths in the MFI system is not fully resolved yet. In the case of pure layered MFI, Zhang *et al.* have suggested the possible connectivities of layered MFI after repetitive branching based upon a hypothesis of their connection by a needle-like MEL domain.[22] Detailed atomic structures of various MFI crystal intergrowth defects have also been suggested.[23]

Fabrication and Characterization of Composite Membranes. The BMLM particles were incorporated in Matrimid, a well-known polyimide membrane material for gas separation applications. The particle/polymer interfacial adhesion in such composite/hybrid membrane materials is a key determinant of the separation performance. The highly roughened surface of BMLM particles is hypothesized to provide a much larger "external" surface area than bare MFI[18] and also would allow penetration of the polymer chains into the mesopores between the layered MFI sheets, thereby allowing much better adhesion than bare MFI. Furthermore, the roughened surfaces have a micropore structure similar to that of the bulk MFI, thereby allowing selective molecular transport through the interfaces.

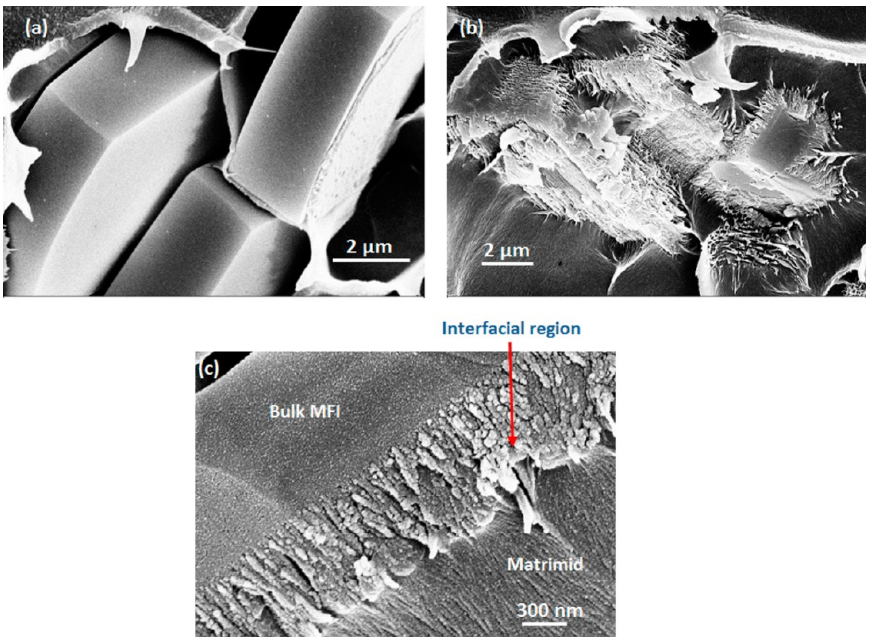

Figure 9. SEM cross-section images of zeolite/Matrimid composite membranes made with (a) bulk MFI and (b, c) BMLM materials. The crystal size of the bulk MFI was 10 μm.

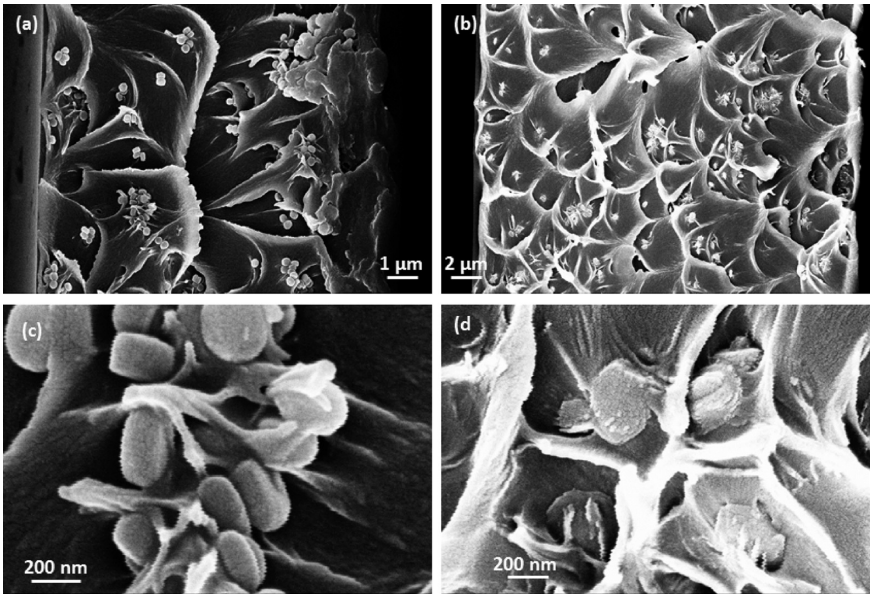

Figure 10. SEM cross-section images of zeolite/Matrimid composite membranes made with (a, c) bare MFI and (b, d) BMLM materials. The crystal size of the bulk MFI was 300 nm.

Figure 9 shows cross-sectional images of the BMLM/Matrimid and bare MFI/Matrimid membranes. To clearly observe the differences in adhesion properties, the larger (10 μm) MFI particles are used. The bare MFI particles (Figure 9a) adhere very poorly to the polymer, leading to macrovoids (~500 nm) at the interfaces. However, the BMLM particles (Figure 9b) show excellent adhesion to the polymer matrix, and no significant voids were detected at the interface. The magnified image at the interfacial region (Figure 9c) shows clear adhesion beween layered MFI and Matrimid. The SEM images indicate penetration of the polymer into the mesoporous spaces between the layered MFI sheets. Figure 10 shows the cross-sectional images of membranes prepared with 300 nm MFI and BMLM particles. In the low-magnification SEM images of Figure 10a, b, the conventional MFI particles were seen to be highly aggregated and poorly adhered to the polymer, whereas the BMLM particles were better dispersed and well-adhered to the polymer. In the magnified SEM images (Figure 10c, d), it is clearly seen that the BMLM particles showed good adhesion to Matrimid,

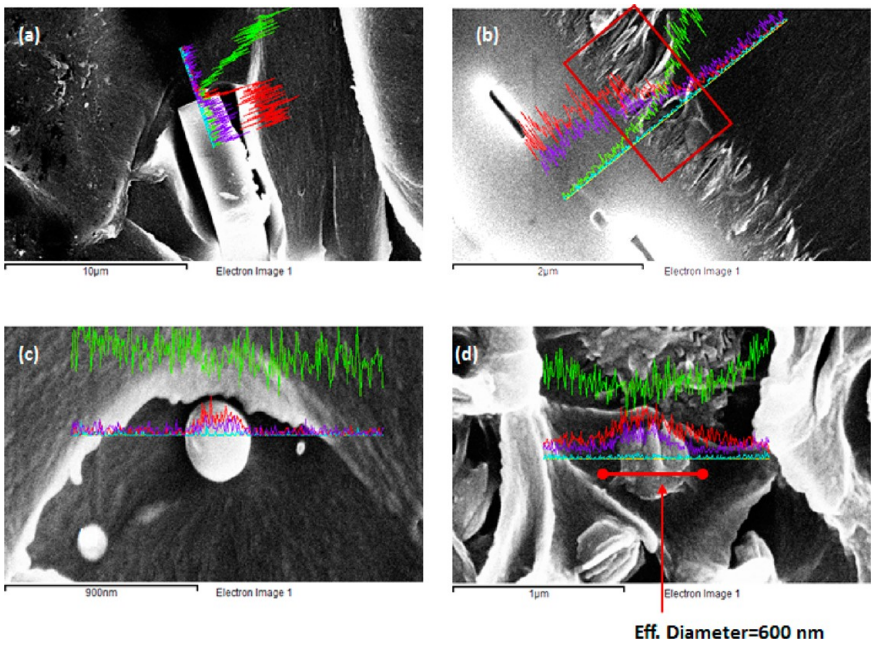

Figure 11. EDX compositional analysis of zeolite/Matrimid composite membranes made with (a, c) bare MFI and (b, d) BMLM materials. The crystal sizes of the bulk MFI were 10 μm (a, c) or 300 nm (b, d). Red, Si; purple, O; green, C; turquoise, N.

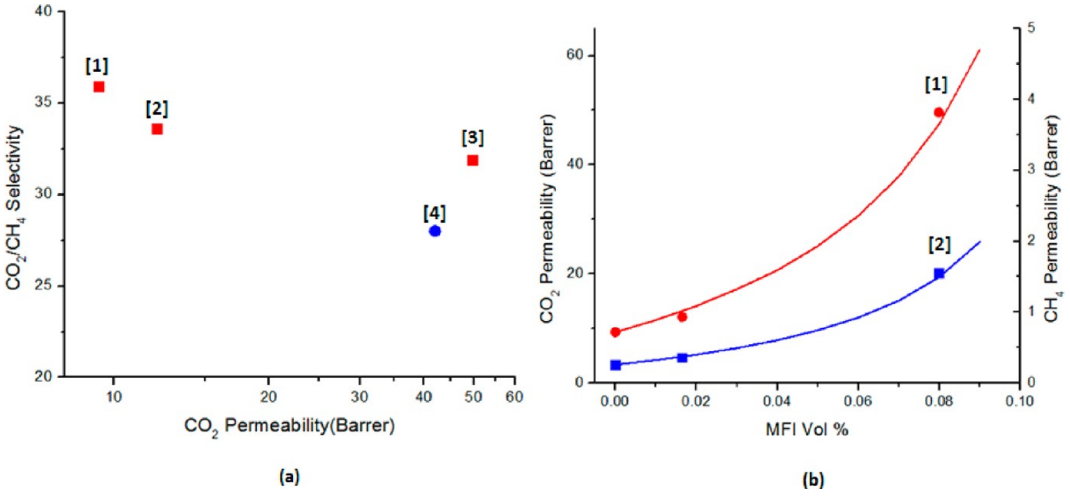

Figure 12. (a) Gas permeation data from [1] bare Matrimid, [2] 5 wt % BMLM composite, [3] 24 wt % BMLM composite, and [4] 20 wt % bulk MFI composite membranes, at 35 °C and 65 psi pressure differential; (b) [1] CO_2 and [2] CH_4 permeabilities (symbols) and fitted prediction by modified Maxwell equations (solid curves).

whereas the bare MFI particles formed macrovoids around aggregated particles.

Figure 11 shows the SEM-EDX carbon and silicon compositional analyses at the BMLM/polymer interfacial region. In contrast with the membranes containing bare MFI particles (Figure 11a, c), the membranes containing BMLM particles (Figure 11b, d) clearly show the interpenetration of the carbon and silicon profiles. Additionally, in Figure 11d the silicon profile around the particle can be used to estimate the effective diameter of BMLM particles in the composite membrane. The EDX-estimated effective diameter of BMLM particles is about 600 nm, which is twice as large as the diameter of the underlying bulk MFI particle (300 nm). Hence, the volume of the interfacial region (including both layered MFI and polymer) is about 7 times larger than the volume of the bulk MFI region and occupies 87.5% of the total particle volume.

CO_2 and CH_4 Gas Permeation. Figure 12a depicts CO_2 permeability and CO_2/CH_4 single-component selectivity of Matrimid membranes incorporating 300 nm bare MFI and the corresponding BMLM material. In the bare MFI composite membranes, the CO_2/CH_4 selectivity was significantly decreased below that of the pure Matrimid membrane. As confirmed from the foregoing discussion, the poor adhesion between the

bare MFI particles and the polymer resulted in the formation of macrovoids, which are possibly also interconnected to allow a continuous nonselective permeation pathway through the membrane.[20] On the other hand, the BMLM composite membrane showed better CO_2/CH_4 separation performance than the conventional MFI composite membrane. The introduction of the highly permeable MFI particles has a large effect on the membrane permeability, and the selectivity is only slightly decreased due to the lower CO_2/CH_4 selectivity of MFI in comparison to Matrimid. This improved separation performance is due to the tight adherence of the BMLM particles to the polymer, caused by infiltration of the polymer into the mesoporous spaces between the layered MFI sheets.

To analyze the dependence of the permeation behavior on the membrane microstructure in more detail, the gas permeation data were fitted to the modified Maxwell equation. In particular, our objective was to estimate the effective particle size and the permeability of the interfacial region. The modified Maxwell equations are given in the Supporting Information (eqs S1−S3) and consider the membrane to have three structural components:[24] the continuous phase (polymer), the bulk dispersed phase (bulk MFI), and an interfacial phase (which in the case of the bare MFI/Matrimid membrane is a void and in the case of the BMLM/Matrimid membrane is the inorganic/polymer interfacial composite region found in Figures 10 and 11). In calculating the effective permeability of the composite membrane, the properties of the interface are represented by the two dimensionless parameters β (ratio of the thickness of the interfacial layer to the radius of the underlying bulk MFI substrate) and γ (ratio of the permeabilities of the interfacial layer and the underlying bulk MFI substrate). The properties of the continuous (polymer) and dispersed (bulk MFI) phases are known from the literature. We used CO_2 (CH_4) permeabilities of 9.33 (0.26) Barrers for Matrimid and 8960 (4032) Barrers for bulk MFI.[25]

For the macrovoids around the bare MFI particles, the gas permeabilities will clearly be close to the Knudsen values of 1 165 849 (1 985 158) Barrers, and therefore we have γ = 130 (479) for CO_2 (CH_4) in this case. However, the modified Maxwell equations (S1−S3) failed to correctly fit the permeability of bare MFI composite membranes for any physically reasonable values of β and γ. It was therefore concluded that in addition to the individual macrovoids present around the bare MFI particles, there is some interconnection of these voids leading to a small but continuous leakage path through the membrane. This feature was added in the form of the leakage fraction χ (eq S4). The values of β and χ were estimated by least-squares fitting. The fitted value of χ was 2×10^{-7}. This very small leakage fraction, in addition to the individual macrovoids, is highly deleterious to the separation performance as seen in Figure 12. The fitted value of β was 0.53. This is quite comparable to the SEM observations, which indicate that the thicknesses of the macrovoids are of the same order of magnitude as the bare MFI particle radius.

In the BMLM/Matrimid composite membranes, there were no macrovoids at the interfacial region, and the polymer chain infiltrates into the mesopores of the layered MFI epitaxially grown at the surface of bare MFI. In this case, the modified Maxwell equation could be applied to estimate the interfacial parameters β and γ. While β is a structural parameter, γ is a permeability parameter and hence differs for the two gases. As a result of the fitting calculations, we obtain the interfacial permeabilities $P_{I,CO2}$ ($P_{I,CH4}$) = 434 (216) Barrers. The interfacial layer is constituted of layered MFI and infiltrated polymer. As expected from such an interfacial layer, the gas permeabilities are intermediate between bulk MFI (several thousand Barrers) and the polymer matrix (<10 Barrers). The fitted β value was estimated as 0.97, which agrees very well with the value of 1.0 obtained from the EDX analysis in Figure 11. Figure 12b shows the individual measured permeabilities of CO_2 and CH_4 in the BMLM/Matrimid composite membranes, along with the modified Maxwell equation predictions using the best fit parameters. This consistent agreement of the gas permeabilities over the range of bulk MFI volume fractions, as well as the excellent agreement of the effective interface thickness, further confirms the good quality of the BMLM/Matrimid composite membranes. The increase in membrane permeability (more than a factor of 5 at 8 vol% loading) upon incorporation of the nanoporous, high-flux BMLM material is much larger than that obtained by incorporating the same loading of nonporous (*e.g.*, TiO_2) nanoparticles into Matrimid (a factor of 1.5−1.7).[26] The latter effect is hypothesized as being caused by disruption of polymer chain packing near the interfaces.[26,27]

CONCLUSION

A new type of hybrid zeolitic material, namely, an overgrowth of layered MFI over a bulk MFI substrate, has been shown. Detailed HRTEM analysis shows epitaxial growth of layered MFI on the bulk MFI substrate in at least two, and possibly all three, principal crystallographic directions. In this "bulk-MFI/layered-MFI" material, the layered MFI creates a large "external surface area" and "surface roughness". The capability of epitaxially growing a layered zeolite on a conventional bulk zeolite creates the possibility of a new class of hybrid zeolitic materials whose properties can be rationally controlled by independently tuning the morphologies of the layered and bulk zeolitic components of the hybrid material. In one example application, we have shown that the highly roughened surface

resulted in excellent adhesion to a dense glassy polymer. BMLM/Matrimid composite membranes showed better gas permeation properties than bare MFI/Matrimid composite membranes, and the fit of the permeation data to the modified Maxwell model yielded physically reasonable values for the interface properties. The BMLM particles are interesting materials for application in molecular separation using composite/hybrid membranes and may also have uses as catalytic materials after substituting some of the Si atoms with Al atoms.

METHODS

Synthesis. Conventional MFI particles of two different sizes (10 μm and 300 nm) were synthesized hydrothermally as described in previous works.[28] The synthesis of the long-chain diquaternary ammonium cation ($C_{22}-N^+-C_6-N^+-C_6$) as a structure-directing agent for layered MFI was carried out as described previously.[11] For comparison with the BMLM material, pure layered MFI was also synthesized as described in previous work.[11,12] The synthesis of BMLM materials was accomplished by the same reaction gel composition used for synthesizing pure layered MFI. However, the bulk MFI particles were added to the gel. In this report, no aluminum source was included in the BMLM synthesis, and a pure-silica hybrid material was obtained. The molar composition of the reaction gel was 30 Na_2O:100 TEOS:10 $C_{22\text{-}6\text{-}6}Br_2$:18 H_2SO_4:70 bulk MFI:4000−16 000 H_2O. The molar quantity of the bulk MFI particles was set to 70% of the dissolved Si source (TEOS). The water content was varied from 4000 to 16 000 to examine the corresponding morphological changes in the BMLM material.

Characterization. Scanning electron microscopy of particles and membranes was performed with a JEOL LEO-1530 operating at 10 kV. Cross sections of membranes were prepared by fracturing the sample in liquid nitrogen. Elemental analysis was performed by SEM-EDX. Samples were gold-coated to prevent surface charging effects. Low-magnification transmission electron microscopy was performed with a Hitachi HF-2000 at 200 kV. High-resolution TEM was performed on a FEI Tecnai G^2 F30 TEM at 300 kV. Typically, the BMLM particles were embedded in epoxy and sliced into 50 nm thin sections by a Leica EM UC6 Ultramicrotome equipped with a diamond knife. Thermogravimetric analysis (TGA) was performed with a Netzsch STA409. The scanning temperature was 30−900 °C at a ramping rate of 10 °C/min, under an N_2:O_2 stream flowing at 90:50 mL/min. N_2 physisorption isotherms were obtained at 77 K with a Micrometrics Tristar II. The samples were degassed for 12 h at 150 °C.

Membrane Fabrication. MFI/Matrimid composite membranes were fabricated *via* a blade-casting method on a glass plate. Dichloromethane (DCM) was used to dissolve the polyimide (Matrimid). For the fabrication of a 20 wt % particle-loaded composite membrane, 0.375 g of particles was dispersed in 8.5 g of DCM and sonicated for 30 min. Then, 1.5 g of Matrimid powder was added and stirred for 1 day using a rotation bar. The dispersion was then sonicated for 30 min to remove any air bubbles. Then, the dispersion was poured on the glass surface and cast using a "doctor's blade" with a height of 12 mils (300 μm). The cast membrane was placed in stagnant air for 1 day and then annealed at 180 °C for 24 h.

Permeation Measurements. The single-component permeabilities of CO_2 and CH_4 were determined using the isochoric (constant-volume, variable-pressure) technique.[29] The upstream pressure was monitored using a 1000 psia Sensotec SC pressure transducer. The pressure in the downstream collection volume was measured using a 10 Torr MKS Baratron (type 127) pressure transducer. The output from the downstream pressure transducer was interfaced with a personal computer using the LabView software for real-time data recording. The entire permeation system was maintained to within ±0.1 °C using a proportional controller (Cole Parmer, BA-2155-54). Several measurements were performed for the thickness of each membrane sample with a micrometer (Ames, Waltham, MA, model #56212) and were then averaged.

Conflict of Interest: The authors declare no competing financial interest.

Acknowledgment. This publication is based on work supported by Award No. KUS-I1-011-21, made by King Abdullah University of Science and Technology (KAUST). M.T. and X.Z. acknowledge support from the Catalysis Center for Energy Innovation (award DESC00001004), an Energy Frontier Research Center funded by the U.S. Department of Energy, Office of Science, Office of Basic Energy Sciences. Portions of this work were conducted at the University of Minnesota Characterization Facility, which receives partial support from the National Science Foundation through the NNIN program. We also thank Prof. W. J. Koros (Georgia Tech) for helpful discussions and for proofreading the manuscript.

Supporting Information Available: SEM and TEM images, XRD patterns, permeation model equations. This material is available free of charge *via* the Internet at http://pubs.acs.org.

REFERENCES AND NOTES

1. Cundy, C. S.; Cox, P. A. The Hydrothermal Synthesis of Zeolites: History and Development from the Earliest Days to the Present Time. *Chem. Rev.* **2003**, *103*, 663–701.
2. Davis, M. E. Zeolite Catalysis: Past, Present, and Future. *Abstr. Pap. Am. Chem. Soc.* **2000**, *219*, U528–U528.
3. Tosheva, L.; Valtchev, V. P. Nanozeolites: Synthesis, Crystallization Mechanism, and Applications. *Chem. Mater.* **2005**, *17*, 2494–2513.
4. Corma, A.; Fornes, V.; Pergher, S. B.; Maesen, T. L. M.; Buglass, J. G. Delaminated Zeolite Precursors as Selective Acidic Catalysts. *Nature* **1998**, *396*, 353–356.
5. Leonowicz, M. E.; Lawton, J. A.; Lawton, S. L.; Rubin, M. K. MCM-22 - A Molecular-Sieve with 2 Independent Multidimensional Channel Systems. *Science* **1994**, *264*, 1910–1913.
6. Corma, A.; Fornes, V.; Diaz, U. ITQ-18 - A New Delaminated Stable Zeolite. *Chem. Commun.* **2001**, *24*, 2642–2643.
7. Kresge, C. T.; Leonowicz, M. E.; Roth, W. J.; Vartuli, J. C.; Beck, J. S. Ordered Mesoporous Molecular-Sieves Synthesized by a Liquid-Crystal Template Mechanism. *Nature* **1992**, *359*, 710–712.
8. Zhao, D. Y.; Feng, J. L.; Huo, Q. S.; Melosh, N.; Fredrickson, G. H.; Chmelka, B. F.; Stucky, G. D. Triblock Copolymer Syntheses of Mesoporous Silica with Periodic 50 to 300 Angstrom Pores. *Science* **1998**, *279*, 548–552.
9. Fan, W.; Snyder, M. A.; Kumar, S.; Lee, P. S.; Yoo, W. C.; McCormick, A. V.; Penn, R. L.; Stein, A.; Tsapatsis, M. Hierarchical Nanofabrication of Microporous Crystals with Ordered Mesoporosity. *Nat. Mater.* **2008**, *7*, 984–991.
10. Choi, M.; Cho, H. S.; Srivastava, R.; Venkatesan, C.; Choi, D. H.; Ryoo, R. Amphiphilic Organosilane-Directed Synthesis of Crystalline Zeolite with Tunable Mesoporosity. *Nat. Mater.* **2006**, *5*, 718–723.
11. Choi, M.; Na, K.; Kim, J.; Sakamoto, Y.; Terasaki, O.; Ryoo, R. Stable Single-Unit-Cell Nanosheets of Zeolite MFI As Active and Long-Lived Catalysts. *Nature* **2009**, *461*, 246–249.
12. Na, K.; Choi, M.; Park, W.; Sakamoto, Y.; Terasaki, O.; Ryoo, R. Pillared MFI Zeolite Nanosheets of a Single-Unit-Cell Thickness. *J. Am. Chem. Soc.* **2010**, *132*, 4169–4177.
13. Na, K.; Jo, C.; Kim, J.; Cho, K.; Jung, J.; Seo, Y.; Messinger, R. J.; Chmelka, B. F.; Ryoo, R. Directing Zeolite Structures into Hierarchically Nanoporous Architectures. *Science* **2011**, *334*, 328–332.
14. Varoon, K.; Zhang, X. Y.; Elyassi, B.; Brewer, D. D.; Gettel, M.; Kumar, S.; Lee, J. A.; Maheshwari, S.; Mittal, A.; Sung, C. Y.; *et al*. Dispersible Exfoliated Zeolite Nanosheets and Their

Application As a Selective Membrane. *Science* **2011**, *333*, 72–75.
15. Nair, S.; Villaescusa, L. A.; Camblor, M. A.; Tsapatsis, M. Zeolite-Beta Grown Epitaxially on SSZ-31 Nanofibers. *Chem. Commun.* **1999**, *10*, 921–922.
16. Okubo, T.; Wakihara, T.; Plevert, J.; Nair, S.; Tsapatsis, M.; Ogawa, Y.; Komiyama, H.; Yoshimura, M.; Davis, M. Heteroepitaxial Growth of a Zeolite. *Angew. Chem., Int. Ed.* **2001**, *40*, 1069–1072.
17. Liu, J. Q.; Bae, T. H.; Esekhile, O.; Nair, S.; Jones, C. W.; Koros, W. J. Formation of $Mg(OH)_2$ Nanowhiskers on LTA Zeolite Surfaces Using a Sol-Gel Method. *J. Sol-Gel Sci. Technol.* **2011**, *60*, 189–197.
18. Bae, T. H.; Liu, J. Q.; Lee, J. S.; Koros, W. J.; Jones, C. W.; Nair, S. Facile High-Yield Solvothermal Deposition of Inorganic Nanostructures on Zeolite Crystals for Mixed Matrix Membrane Fabrication. *J. Am. Chem. Soc.* **2009**, *131*, 14662–14663.
19. Lydon, M. E.; Unocic, K. A.; Bae, T. H.; Jones, C. W.; Nair, S. Structure-Property Relationships of Inorganically Surface-Modified Zeolite Molecular Sieves for Nanocomposite Membrane Fabrication. *J. Phys. Chem. C* **2012**, *116*, 9636–9645.
20. Chaidou, C. I.; Pantoleontos, G.; Koutsonikolas, D. E.; Kaldis, S. P.; Sakellaropoulos, G. P. Gas Separation Properties of Polyimide-Zeolite Mixed Matrix Membranes. *Sep. Sci. Technol.* **2012**, *47*, 950–962.
21. Diaz, I.; Kokkoli, E.; Terasaki, O.; Tsapatsis, M. Surface Structure of Zeolite (MFI) Crystals. *Chem. Mater.* **2004**, *16*, 5226–5232.
22. Zhang, X. Y.; Liu, D. X.; Xu, D. D.; Asahina, S.; Cychosz, K. A.; Agrawal, K. V.; Al Wahedi, Y.; Bhan, A.; Al Hashimi, S.; Terasaki, O.; *et al*. Synthesis of Self-Pillared Zeolite Nanosheets by Repetitive Branching. *Science* **2012**, *336*, 1684–1687.
23. Ramsahye, N. A.; Slater, B. Incidence and Properties of Nanoscale Defects in Silicalite. *Chem. Commun.* **2006**, *4*, 442–444.
24. Mahajan, R.; Koros, W. J. Mixed Matrix Membrane Materials with Glassy Polymers. Part 1. *Polym. Eng. Sci.* **2002**, *42*, 1420–1431.
25. Kusakabe, K.; Yoneshige, S.; Murata, A.; Morooka, S. Morphology and Gas Permeance of ZSM-5-Type Zeolite Membrane Formed on a Porous Alpha-Alumina Support Tube. *J. Membr. Sci.* **1996**, *116*, 39–46.
26. Moghadam, F.; Omidkhah, M. R.; Vasheghani-Farahani, E.; Pedram, M. Z.; Dorosti, F. The Effect of TiO_2 Nanoparticles on Gas Transport Properties of Matrimid5218-Based Mixed Matrix Membranes. *Sep. Purif. Technol.* **2011**, *77*, 1218–136.
27. Merkel, T. C.; Freeman, B. D.; Spontak, R. J.; He, Z.; Pinnau, I.; Meakin, P.; Hill, A. J. Ultrapermeable, Reverse-Selective Nanocomposite Membranes. *Science* **2002**, *296*, 519–522.
28. Hsu, C. Y.; Chiang, A. S. T.; Selvin, R.; Thompson, R. W. Rapid Synthesis of MFI Zeolite Nanocrystals. *J. Phys. Chem. B* **2005**, *109*, 18804–18814.
29. Lee, J. S.; Madden, W.; Koros, W. J. Antiplasticization and Plasticization of Matrimid Asymmetric Hollow Fiber Membranes-Part A. Experimental. *J. Membr. Sci.* **2010**, *350*, 232–241.